PNAS RESEARCH ARTICLE | BIOCHEMISTRY

In transcription antitermination by Qλ, NusA induces refolding of Qλ to form a nozzle that extends the RNA polymerase RNA-exit channel

Zhou Yin[a,b], Jeremy G. Bird[a,b,c], Jason T. Kaelber[d], Bryce E. Nickels[a,c], and Richard H. Ebright[a,b,1]

Edited by Jeffrey Roberts, Cornell University, Ithaca, NY; received March 25, 2022; accepted July 8, 2022

Lambdoid bacteriophage Q proteins are transcription antipausing and antitermination factors that enable RNA polymerase (RNAP) to read through pause and termination sites. Q proteins load onto RNAP engaged in promoter-proximal pausing at a Q binding element (QBE) and adjacent sigma-dependent pause element to yield a Q-loading complex, and they translocate with RNAP as a pausing-deficient, termination-deficient Q-loaded complex. In previous work, we showed that the Q protein of bacteriophage 21 (Q21) functions by forming a nozzle that narrows and extends the RNAP RNA-exit channel, preventing formation of pause and termination RNA hairpins. Here, we report atomic structures of four states on the pathway of antitermination by the Q protein of bacteriophage λ (Qλ), a Q protein that shows no sequence similarity to Q21 and that, unlike Q21, requires the transcription elongation factor NusA for efficient antipausing and antitermination. We report structures of Qλ, the Qλ-QBE complex, the NusA-free pre-engaged Qλ-loading complex, and the NusA-containing engaged Qλ-loading complex. The results show that Qλ, like Q21, forms a nozzle that narrows and extends the RNAP RNA-exit channel, preventing formation of RNA hairpins. However, the results show that Qλ has no three-dimensional structural similarity to Q21, employs a different mechanism of QBE recognition than Q21, and employs a more complex process for loading onto RNAP than Q21, involving recruitment of Qλ to form a pre-engaged loading complex, followed by NusA-facilitated refolding of Qλ to form an engaged loading complex. The results establish that Qλ and Q21 are not structural homologs and are solely functional analogs.

transcription antitermination | RNA polymerase | transcription elongation complex | transcription antitermination factor Qλ | transcription antitermination factor Q21

Significance

Bacteriophage Q proteins are textbook examples of regulators of gene expression that function through transcription antitermination. Here, we report structures that define the mechanism of antitermination by the Q protein of bacteriophage λ (Qλ). The results show Qλ forms a nozzle that narrows and extends the RNA polymerase RNA-exit channel, precluding the formation of terminator RNA hairpins. The results show Qλ exhibits no structural similarity to the previously characterized Q protein of bacteriophage 21 (Q21), employs a different mechanism for DNA binding than Q21, and employs a more complex process of loading onto RNA polymerase than Q21. We conclude Qλ and Q21 are not structural homologs and are solely functional analogs, akin to a bird wing and a bat wing.

Lambdoid bacteriophage Q proteins are transcription antitermination and antipausing factors that enable RNA polymerase (RNAP) to read through pause and termination sites [(1–7), reviewed in (8–10)]. Q proteins load onto transcription elongation complexes (TECs) engaged in promoter-proximal pausing to yield Q-loading complexes, and Q proteins subsequently translocate with TECs as pausing-deficient, termination-deficient Q-loaded complexes (3–10).

The Q-dependent gene regulatory cassette consists of the gene for Q, followed by a transcription unit comprising a promoter (PR′), a promoter-proximal σ-dependent pause element (SDPE), a terminator, and downstream genes [Fig. 1*A* (3–10)]. In the absence of Q, RNAP initiating transcription at the PR′ promoter pauses at the SDPE and terminates at the terminator, and, as a result, fails to transcribe downstream genes. In the presence of Q, RNAP initiating at the PR′ promoter rapidly escapes the SDPE and reads through the terminator, and, as a result, transcribes downstream genes (3–10). Q functions at the Q-dependent gene regulatory cassette by first forming a Q-loading complex, comprising a Q protein bound to a Q binding element (QBE) and a σ-containing TEC paused at the SDPE (Fig. 1*B*, lines 1–4), and then forming a Q-loaded complex, comprising a Q-containing TEC that processively, over thousands of base pairs, ignores pause and termination sites [Fig. 1*B*, line 5 (3–11)].

Q proteins comprise three protein families: the Q21 family [Pfam PF06530; 5,251 entries in National Center for Biotechnology Information data bank (NCBI)], the Qλ family (Pfam PF03589, 7,904 entries in NCBI), and the Q82 family (Pfam PF06323, 2,635 entries in NCBI) (12). Q proteins from the three protein families exhibit equivalent antitermination and antipausing activities, perform equivalent regulatory functions, and are encoded by genes that exhibit equivalent positions in bacteriophage genomes (8, 12–15), but Q proteins from the three protein families exhibit no obvious sequence similarity (8, 12–15). This raises the question of whether Q proteins from the three families

Author affiliations: [a]Waksman Institute, Rutgers University, Piscataway, NJ 08854; [b]Department of Chemistry and Chemical Biology, Rutgers University, Piscataway, NJ 08854; [c]Department of Genetics, Rutgers University, Piscataway, NJ 08854; and [d]Rutgers Cryo-EM and Nanoimaging Facility, Rutgers University, Piscataway, NJ 08854

Author contributions: Z.Y. and R.H.E. designed research; Z.Y., J.G.B., and J.T.K. performed research; Z.Y., B.E.N., and R.H.E. analyzed data; and Z.Y., B.E.N., and R.H.E. wrote the paper.

The authors declare no competing interest.

This article is a PNAS Direct Submission.

See online for related content such as Commentaries.

[1]To whom correspondence may be addressed. Email: ebright@waksman.rutgers.edu.

This article contains supporting information online at http://www.pnas.org/lookup/suppl/doi:10.1073/pnas.2205278119/-/DCSupplemental.

Published August 11, 2022.

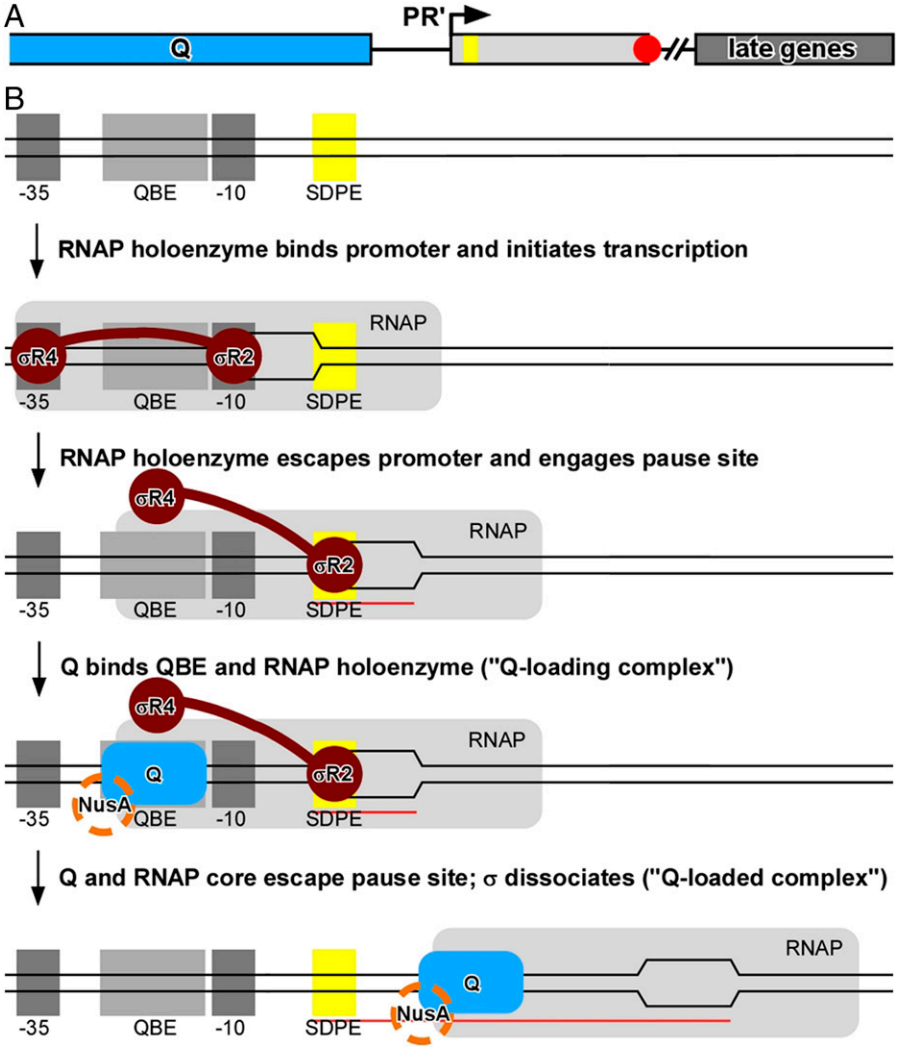

Fig. 1. Biological function of Q. (*A*) Q-dependent regulatory cassette, consisting of the gene for Q (blue) and an adjacent transcription unit comprising the PR′ promoter (arrow), SDPE (yellow rectangle), terminator (red octagon), and bacteriophage late genes (dark gray). (*B*) Steps in assembly and function of a Q-dependent transcription antitermination complex. Promoter -35 and -10 elements, dark gray rectangles; QBE, light gray rectangle; SDPE, yellow rectangle; RNAP core enzyme, light gray; σ, brown; Q, blue; NusA [needed for efficient antitermination by Qλ and Q82 (2, 4, 51, 52)], orange; DNA nontemplate and template strands, black lines (unwound transcription bubble indicated by raised and lowered line segments); RNA, red line.

possess three-dimensional structural homology, despite the absence of obvious sequence similarity, or lack three-dimensional structural homology and are solely functional analogs (akin to a bird wing, a bat wing, and a fly wing).

We recently reported a set of structures that defined the structural basis of antitermination and antipausing by the Q protein of lambdoid bacteriophage 21 (Q21): i.e., Q21, the Q21-QBE complex, the Q21-loading complex, and the Q21-loaded complex [(12), see also (16)]. In the Q21-QBE complex, two Q21 protomers interact with two tandem, directly repeated, DNA subsites (12, 16). In the Q21-loading complex, one of the two Q21 protomers that interacts with the QBE also interacts with a σ-containing TEC, forming a "Q torus," or "Q nozzle," that narrows and extends the RNAP RNA-exit channel (12, 16). In the Q21-loaded complex, the nascent RNA product threads through the Q nozzle, preventing the formation of pause and termination RNA hairpins, and topologically linking Q to the TEC, yielding an essentially unbreakable, processively acting, antipausing and antitermination complex (12, 16).

Here, we report a set of structures that define the structural basis of antitermination by the Q protein of bacteriophage λ (Qλ): i.e., a crystal structure of Qλ, a crystal structure of a Qλ-QBE complex, a cryogenic electron microscopy (cryo-EM) structure of a "pre-engaged" Qλ-loading complex, and a cryo-EM structure of a NusA-containing "engaged" Qλ-loading complex. The results reveal that Qλ, like Q21, forms a nozzle that narrows and extends the RNAP RNA-exit channel. The results further reveal that the three-dimensional structures, the mechanisms of QBE recognition, and the mechanisms of Q loading differ for Qλ and Q21, and thus that Qλ and Q21 are not structural homologs and are solely functional analogs (akin to a bird wing and a bat wing).

Results

Structure of Qλ. In previous work, we determined a crystal structure at a 2.1-Å resolution of a Qλ fragment lacking part of the 60-residue intrinsically disordered N-terminal segment of Qλ [$Q\lambda^{39–207}$ (17)]. In the present work, we have determined crystal structures that have higher resolutions (1.46 Å for a crystal structure in the same crystal form and 1.97 Å for a crystal structure in a new crystal form) of a Qλ fragment lacking the entire 60-residue, intrinsically disordered N-terminal segment and that have the E134K substitution, which previously has been shown to increase Qλ-QBE binding affinity [$Q\lambda^{61–207;N61S;E134K}$ (18); Fig. 2 and *SI Appendix*, Table S1].

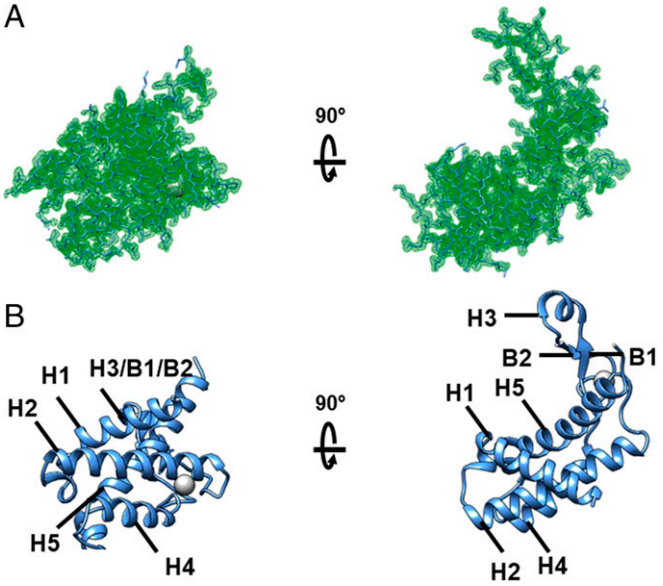

Fig. 2. Structure of Qλ. (*A*) Type I crystal structure; two orthogonal views. Experimental electron density map (green mesh, 2mFo-DFc map contoured at 1.0σ) and fitted atomic model (blue). The Qλ body comprises α-helices 1, 2, 4, and 5 (H1, H2, H4, and H5). The Qλ arm comprises α-helix 3 and β-strands 1 and 2 (H3, B1, and B2). The Qλ HTH motif comprises H4 and H5. (*B*) Type I crystal structure with ribbon representation; two orthogonal views. Zn^{2+}, gray sphere.

The new structures confirm that Qλ comprises a four-helix-bundle globular domain containing a canonical helix-turn-helix (HTH) DNA binding motif ("Qλ body"; residues 61 to 113 and 153 to 207) and a type I shuffled (19) zinc ribbon ("Qλ arm"; residues 114 to 152; Fig. 2). The new structures also confirm that Qλ exhibits no three-dimensional structural similarity to Q21, apart from the presence in Qλ of a canonical HTH motif and presence in Q21 of a noncanonical, interrupted helix-turn-loop-helix motif (12, 16).

Structure of Qλ-QBE Complex. We have determined a crystal structure of the Qλ-QBE complex at a 2.18-Å resolution by use of single-wavelength anomalous dispersion ($Q\lambda^{61–207;N61S;E134K}$-QBE; Fig. 3 and *SI Appendix*, Fig. S1 and Table S1). The structure shows that Qλ interacts as a monomer, in an extended conformation, with a DNA site that spans more than one turn of DNA (13 bp; Fig. 3 and *SI Appendix*, Fig. S1*A*). The Qλ body interacts, through its HTH motif, with the DNA major groove at positions 1 to 4 of the DNA site (Fig. 3 *A*, *B*, *D*, and *E*), and the Qλ arm interacts, through residues close to the residues that coordinate the Zn^{2+} ion of its zinc ribbon, with the DNA major groove at positions 11 to 13 of the DNA site (Fig. 3 *A*, *B*, and *F*). The observed interactions are consistent with, and account for, genetic and biochemical results defining Qλ and QBE determinants for Qλ-QBE interaction [*SI Appendix*, Fig. S1*A* (4, 18, 20)]. The E134K substitution that increases DNA binding affinity (18) replaces a negatively charged residue of the Qλ arm tip that is predicted to be 5 Å from the negatively charged DNA-phosphate backbone with a positively charged residue, thus replacing an unfavorable electrostatic protein-DNA interaction with a favorable electrostatic interaction (*SI Appendix*, Fig. S1*B*).

Comparison of the structures of Qλ-QBE and Qλ shows that in Qλ-QBE, the Qλ arm is rotated through an ∼75° swinging motion, resulting in a substantially more extended conformation (∼40 Å more extended for the Qλ arm tip) able to interact with a DNA site that spans more than one turn of DNA (Fig. 3*C*, blue vs. gray ribbons). The structures suggest that formation of Qλ-QBE may involve two steps: a first step in which the Qλ body interacts with positions 1 to 4 of the QBE, and a second step in which the Qλ arm rotates, through an ∼75° swinging motion, to interact with positions 11 to 13 of the DNA site (Movie S1).

The structure of the Qλ-QBE complex, in which Qλ interacts as an extended monomer with a non-repeat, asymmetric DNA site (Fig. 3 *A*–*C*), is radically different from the structure of the Q21-QBE complex, in which Q21 interacts as a dimer with a direct-repeat DNA site (12, 16). The results provide further evidence that Qλ and Q21 are not structural homologs.

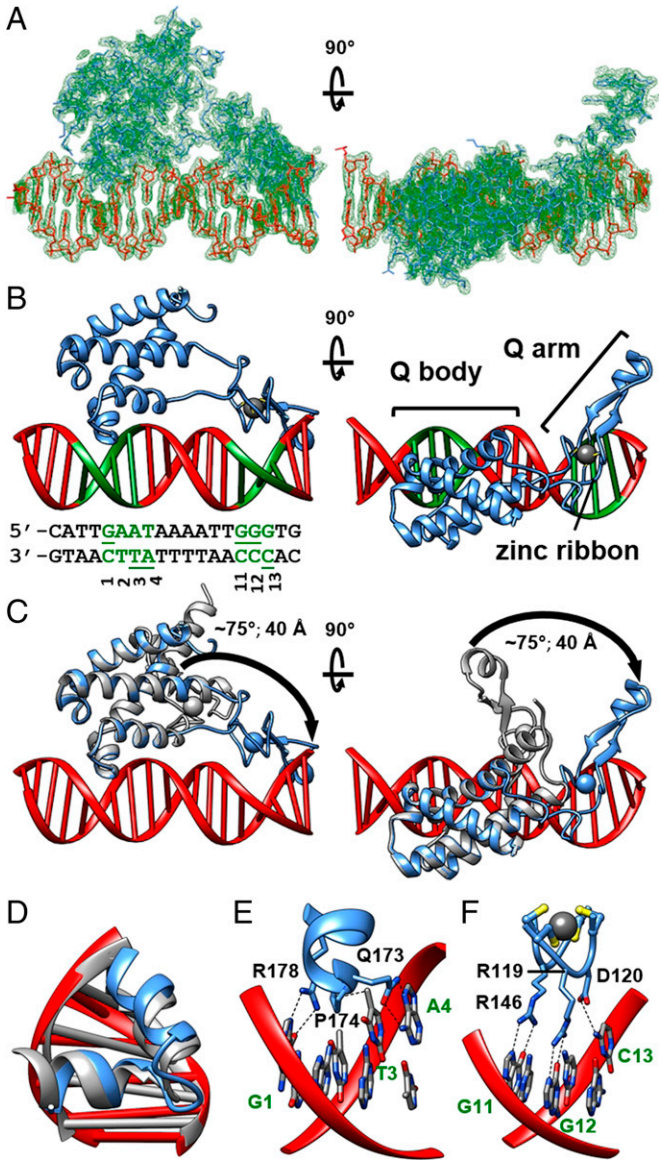

Fig. 3. Structure of the Qλ-QBE complex. (*A*) Two orthogonal views. Experimental electron density map (green mesh, 2mFo-DFc map contoured at 1.0σ) and fitted atomic model (red and blue). (*B*) Ribbon representation; two orthogonal views. Red and green show the QBE DNA fragment (nucleotide pairs 1 to 4 and 11 to 13 in green; contacted bases underlined). Other colors are as in Fig. 2*B*. (*C*) Superimposition of the structure of Qλ (type I crystal structure; gray ribbon; gray sphere for associated Zn^{2+}) on the structure of the Qλ-QBE complex (blue and red ribbons for Qλ and QBE; blue sphere for associated Zn^{2+}). (*D*) Qλ HTH motif (blue) interacting with DNA (red) superimposed on the λ Cro HTH motif interacting with DNA [Protein Data Bank (PDB): 6CRO (56); gray]. (*E*) Interactions of the Qλ body with the DNA major groove of nucleotide pairs 1 to 4. (*F*) Interactions of the Qλ arm with the DNA major groove of nucleotide pairs 11 to 13.

Structure of Pre-Engaged Qλ-Loading Complex. We have determined a single-particle reconstruction cryo-EM structure of a Qλ-loading complex at a 3.13-Å resolution (Fig. 4 and *SI Appendix*, Figs. S2 and S3 and Table S2). We prepared the Qλ-loading complex by in vitro reconstitution from full-length Qλ, *Escherichia coli* RNAP core, an *E. coli* σ^{70} derivative with substitutions that increase the efficiency of Qλ loading [R541C and L607P (21–23)], and a nucleic-acid scaffold containing the λPR′ QBE, a consensus version of the λPR′ SDPE, and an 11-nt RNA (Fig. 4*A*). The DNA duplex contained a 16-bp non-complementary region overlapping the SDPE, corresponding to the unwound and scrunched transcription bubble in the Qλ-free, σ-containing paused TEC (pTEC) at λPR′ (24).

The structure shows Qλ interacting with the QBE in a manner matching that in the crystal structure of Qλ-QBE (Fig. 4*B* vs. Fig. 3*A*) and simultaneously interacting with a σ-containing pTEC (Fig. 4*B*). The structural module of σ that recognizes the promoter -10 element in a transcription initiation complex, σ region 2 (σR2), makes interactions with the SDPE -10-element-like sequence and RNAP equivalent to those it makes in a transcription initiation complex (Fig. 4*B*). In contrast, the structural module of σ that recognizes a promoter -35 element in a transcription initiation complex, σ region 4 (σR4), makes interactions radically different from those it makes in a transcription initiation complex. In a transcription initiation complex, σR4 interacts with the RNAP flap-tip helix [FTH; β residues 897 to 907 (25–28)] and interacts with a -35 element ∼17 bp upstream of σR2 bound to a -10 element (27, 29–31). In the Qλ-containing pTEC, σR4 is disengaged from the RNAP FTH and is repositioned to a -35-element-like DNA site immediately upstream of σR2 bound to the SDPE -10-element-like sequence, where it makes protein-DNA interactions essentially identical to those it makes with a promoter -35 element in a transcription initiation complex (Fig. 4 *B* and *C* and *SI Appendix*, Fig. S4), consistent with published genetic and biochemical data (22, 32–34). The repositioned σR4 makes protein-protein interactions with Qλ

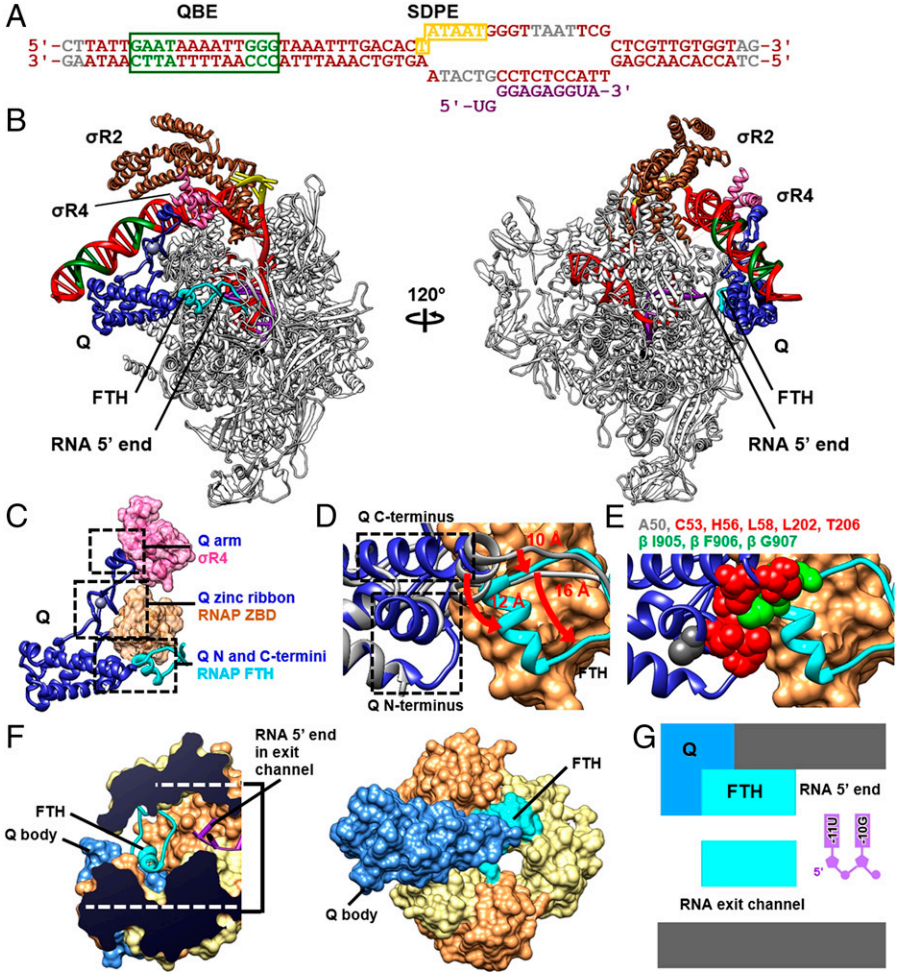

Fig. 4. Structure of the pre-engaged Qλ-loading complex. (*A*) Nucleic-acid scaffold. DNA, red (QBE nucleotide pairs 1 to 4 and 11 to 13, SDPE, and disordered nucleotides in green, yellow, and gray, respectively; non-complementary region corresponding to the unwound transcription bubble indicated by raised and lowered letters); RNA, magenta. (*B*) Overall structure (two view orientations). Qλ, blue; RNAP, gray; RNAP FTH and connecting segments, cyan; σR2, brown; σR4, pink; DNA and RNA, colored as in *A*; RNAP active-center Mg^{2+}, black sphere. (*C*) Qλ-RNAP interactions. Qλ, blue; RNAP ZBD, salmon. Other colors and view orientation are as in *B*, *Left*. (*D*) Conformational changes in Qλ upon formation of the pre-engaged Qλ-loading complex. Qλ in the Qλ-QBE complex (Fig. 3 *B*, *Left*; gray) is superimposed on Qλ in the pre-engaged Qλ-loading complex (colored as in *B* and *C*). Dashed rectangles, Qλ N-terminal residues that fold and C-terminal residues that refold upon formation of the pre-engaged Qλ-loading complex (residues 46 to 60 and 195 to 207). (*E*) Interactions of the Qλ N- and C-terminal segments with RNAP FTH in the pre-engaged Qλ-loading complex. Sites of substitutions of Qλ that result in defects in Qλ-dependent antitermination but not Qλ-QBE interaction (35) are shown in red (residues that interact with FTH: C53, H56, L58, L202, and T206) and gray (residue that does not interact with FTH: A50). Sites of substitutions of FTH that result in defects in Qλ-dependent antitermination and Qλ-FTH interaction (23) are shown in green (I905, F906, and G907). View orientation is as in *D*. (*F*) Qλ (blue) outside the RNAP RNA-exit channel, RNAP FTH (cyan) partly in the RNAP RNA-exit channel, and RNA (magenta; numbered to assign the RNA 3′ nucleotide as -1) in the RNAP RNA-exit channel. RNAP β and β′ are in salmon and light yellow, respectively. *Left:* View orientation is orthogonal to the RNA-exit channel. *Right:* View orientation is parallel to the RNA-exit channel. (*G*) Summary of organization of Qλ (blue), RNAP FTH (cyan), the RNAP RNA-exit channel (gray), and RNA (magenta). View orientation is as in *F*, *Left*.

(with the N-terminal part of σR4, residues 552 to 554, interacting with the Qλ arm tip, residues 133 to 137; Fig. 4 *B* and *C* and *SI Appendix*, Fig. S4), consistent with genetic and biochemical data indicating the importance of Qλ residue 134 and σ residue 553 for Qλ-σR4 interaction [Fig. 4 *B* and *C* and *SI Appendix*, Fig. S4*A* (17, 33)]. The repositioned σR4 also makes unanticipated protein-protein interactions with σR2 (with the C-terminal part of σR4, residues 595 and 599, interacting with the σR2 nonconserved region, residues 154 to 155; Fig. 4 *B* and *C* and *SI Appendix*, Fig. S4*B*). The structural modules of σ between σR2 and σR4, σ region 3 (σR3) and the σR3-σR4 linker, are disengaged from their positions in a transcription initiation complex—where σR3 interacts with DNA immediately upstream of σR2 bound to a -10 element, and where the σR3-σR4 linker occupies the RNAP RNA-exit channel (27, 30, 31)—and are disordered (Fig. 4*B*). Clear, traceable density is present for the entire 11-nt RNA. The RNA 5′-end nucleotide and one additional RNA nucleotide (positions -11 and -10) are in the RNAP RNA-exit channel, and the other nine RNA nucleotides (position -9 through -1) are base paired to the transcription-bubble template DNA strand as an RNA-DNA hybrid (Fig. 4*B*).

Comparison of the structure of the Qλ-containing pTEC at λPR′ (Fig. 4) to the structure of the Qλ-free pTEC at λPR′ (24) reveals four structural changes induced by Qλ: 1) repositioning of σR4 to the DNA segment immediately upstream of σR2, 2) displacement of σR3 from the DNA segment immediately upstream of σR2, 3) bending of upstream DNA by ∼40° toward the RNAP zinc binding domain (ZBD), and 4) repositioning of the RNAP FTH and the protein segments that precede and follow it, by 10 to 16 Å, into the RNAP RNA-exit channel. The first of these structural changes is induced directly by Qλ, through direct Qλ-σR4 interaction (Fig. 4 *B* and *C* and *SI Appendix*, Fig. S4). The second is induced indirectly, by the repositioning of σR4 to the DNA segment immediately upstream of σR4 (Fig. 4*B*). The third and fourth are induced directly, through direct Qλ-ZBD and Qλ-FTH interactions (Fig. 4 *B*–*E*).

Comparison of the structure of the Qλ-containing pTEC (Fig. 4) to the structure of the Qλ-QBE complex (Fig. 3) reveals that, upon interaction with the pTEC: 1) 16 residues of the 60-residue intrinsically disordered N-terminal segment of Qλ undergo a disorder-to-order transition, folding as a turn followed by an α-helix (residues 45 to 60; Fig. 4*D* and Movie S2), and 2) 12 residues of the C-terminal segment of Qλ refold, extending the C-terminal α-helix of Qλ by three turns (residues 195 to 207; Fig. 4*D* and Movie S2).

In addition to interacting with, and repositioning, σR4 (Fig. 4 *B* and *C* and *SI Appendix*, Fig. S4), Qλ interacts with RNAP in the Qλ-containing pTEC (Fig. 4 *B*–*E*). The Qλ zinc ribbon (residues 110 to 112, 117, and 122 to 126) interacts with the RNAP ZBD (β′ residues 75, 82 to 86, and 91; Fig. 4*C*), and the Qλ N-terminal and C-terminal regions (residues 52, 56, 58, 202, and 206) interact with the C-terminal half of the RNAP FTH (β residues 905 to 906; Fig. 4*E*). There is a nearly one-for-one correspondence between Qλ residues observed to make Qλ-FTH interactions in the structure and Qλ residues shown experimentally to be important for Qλ-dependent antitermination but not for Qλ-QBE interaction [Fig. 4*E*, red (35)], suggesting that the observed interactions are functionally relevant. Furthermore, there is a one-for-one correspondence between RNAP FTH residues observed to make Qλ-FTH interactions in the structure and FTH residues previously shown experimentally to be important for Qλ-dependent antitermination and Qλ-FTH interaction [Fig. 4*E*, green (23)], further suggesting that the observed interactions are functionally relevant.

In the Qλ-containing pTEC, Qλ-FTH interactions reposition part of the RNAP FTH into the RNAP RNA-exit channel (Fig. 4 *F* and *G*). However, in contrast to the structure of the Q21-loading complex—in which Q21 forms a torus at the mouth of, and inside of, the RNAP RNA-exit channel that narrows and extends the RNAP RNA-exit channel (12, 16)—in the structure of this Qλ-containing pTEC, Qλ does not interact with, or enter, the RNAP RNA-exit channel (Fig. 4 *F* and *G*).

We term the structural state in Fig. 4 the "Qλ 'pre-engaged' loading complex" to reflect the fact that this structural state has Qλ recruited to the pTEC but does not have Qλ interacting with, or entering, the RNAP RNA-exit channel.

Structure of NusA-Containing Engaged Qλ-Loading Complex. Qλ requires the transcription elongation factor NusA (10, 36, 37) for efficient antitermination (2, 4). NusA stabilizes the Qλ-loading complex (4) and increases the antitermination activity of the Qλ-loaded complex (2, 4). We have determined a single-particle reconstruction cryo-EM structure of a NusA-containing Qλ-loading complex, prepared as in the preceding section, but in the presence of NusA, at a 3.36-Å resolution (Fig. 5 and *SI Appendix*, Figs. S5 and S6 and Table S2).

The NusA-containing Qλ-loading complex (Fig. 5) has the same overall structural organization as the NusA-free, pre-engaged Qλ-loading complex (Fig. 4). Qλ interacts with the QBE through the Qλ body and Qλ arm and simultaneously interacts with a σ-containing pTEC, with the Qλ body interacting with the RNAP ZBD and the Qλ arm tip interacting with σR4 repositioned to the DNA segment immediately upstream of σR2 bound to the SDPE -10-like element (Fig. 5 *A* and *B*).

In the NusA-containing Qλ-loading complex, NusA interacts with both RNAP and Qλ (Fig. 5*A* and *SI Appendix*, Fig. S7). The NusA N-terminal domain interacts with the RNAP FTH and with one RNAP α-subunit C-terminal domain, making interactions equivalent to those it makes in other structures of NusA-containing TECs [Fig. 5*A* and *SI Appendix*, Fig. S7 (38–44)]. The NusA S1 domain (residues 144 to 147 and 170 to 175) interacts with the Qλ body (residues 80 to 81, 106 to 107, and 182 to 197) (Fig. 5*A* and *SI Appendix*, Fig. S7).

Comparison of the structure of the NusA-containing Qλ-loading complex (Fig. 5) to the structure of the NusA-free, pre-engaged Qλ-loading complex (Fig. 4) shows that upon binding of NusA, remarkable large-scale conformational changes occur in the RNAP FTH and in Qλ. The RNAP FTH, which interacts with Qλ in the NusA-free, pre-engaged Qλ-loading complex (Fig. 4), moves by 26 Å, breaking its interactions with Qλ and, instead, making interactions with the NusA N-terminal domain (Fig. 5*A* and *SI Appendix*, Fig. S7). Residues 1 to 44 of Qλ, which are disordered in Qλ, in Qλ-QBE, and in the NusA-free, preengaged Qλ-loading complex (Figs. 3 and 4), undergo a disorder-to-order transition to form a Qλ torus and to position the Qλ torus at the mouth of, and inside, the RNAP RNA-exit channel, in space vacated by the repositioned RNAP FTH (Fig. 5 and Movie S3). Residues 1 to 44 of Qλ fold to form a first α-helix, followed by a loop, followed by a second α-helix (residues 1 to 11, 12 to 31, and 32 to 42, respectively). The first α-helix interacts with residues of the RNAP ZBD at the mouth of the RNA-exit channel (β′ residues 67, 78 to 79, 94, and 96), the loop interacts with residues of the RNAP ZBD (β′ residue 49) and RNAP flap (β residues 843 to 844, 848, 888, 914 to 917, and 919) inside the RNA-exit channel,

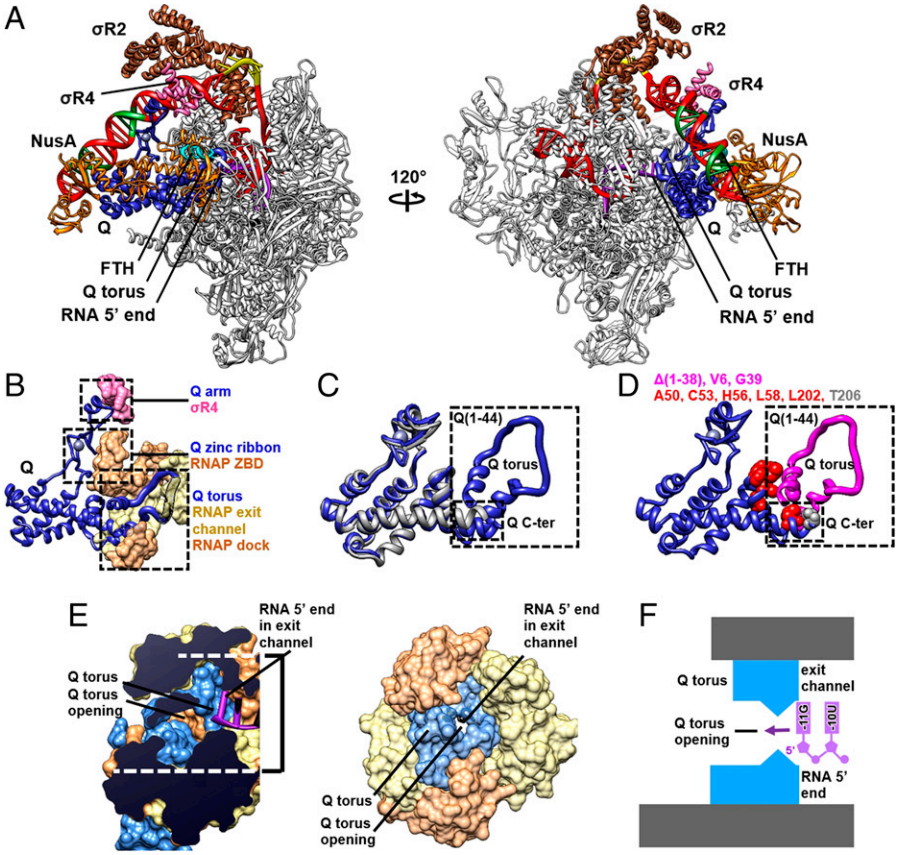

Fig. 5. Structure of the NusA-containing engaged Qλ-loading complex. (*A*) Overall structure. NusA, orange. View orientations and other colors are as in Fig. 4*B*. (*B*) Qλ-RNAP interactions. Qλ, blue, with segments located inside the RNAP RNA-exit channel, behind RNAP surfaces, indicated as gray ribbons with black outlines. RNAP β and β′, salmon and light yellow, respectively. NusA is omitted for clarity. Other colors and view orientation are as in Fig. 4*C*. (*C*) Conformational changes in Qλ upon formation of the NusA-containing engaged Qλ-loading complex. Qλ in the pre-engaged Qλ-loading complex (Fig. 4 *B*, *Left*; gray) is superimposed on Qλ in the NusA-containing engaged Qλ-loading complex (colored as in *A* and *B*). Large dashed rectangle, Qλ N-terminal residues that fold to form the Qλ torus (residues 1 to 44). Small dashed rectangle, Qλ C-terminal residues that interact with the N-terminal region of the Qλ torus. (*D*) Formation of the Qλ torus at and inside the RNAP RNA-exit channel in the NusA-containing engaged Qλ-loading complex. Qλ residues deleted in mutant defective in Qλ-dependent antitermination but not defective in Qλ-QBE interaction [residues 1 to 38 (17)] and Qλ residues altered in single-substitution mutants defective in Qλ-dependent antitermination but not defective in Qλ-QBE interaction [V6A and G39A (35)] are shown as pink ribbons and pink surfaces, respectively. Sites of substitutions of Qλ that result in defects in Qλ-dependent antitermination but not Qλ-QBE interaction (35) are shown in red (residues that interact with the Qλ torus: C53, H56, L58, L202, and T206) and gray (residue that does not interact with the Qλ torus: T206). View orientation and dashed rectangles are as in *C*. (*E*) Restriction of the RNAP RNA-exit channel by the Qλ torus (blue) and proximity of the RNA 5′ end (magenta; RNA nucleotides numbered to assign the RNA 3′ nucleotide as -1) to the Qλ torus. RNAP β and β′, salmon and light yellow, respectively. *Left:* View orientation orthogonal to the RNA-exit channel. *Right:* View orientation parallel to the RNA-exit channel. (*F*) Summary of organization of the Qλ torus (blue), RNAP RNA-exit channel (gray), and RNA (magenta). View orientation is as in *E*, *Left*. During transcription, as the RNA product is extended from 11 nt (as in this structure) to 12 nt, from 12 nt to 14 nt, and from 14 nt to 15 or 16 nt, the RNA 5′ end is anticipated to thread into, through, and outside, respectively, the Qλ torus.

and the second α-helix interacts with residues of the RNAP dock (β′ residues 386, 394, and 397 to 398) and RNAP β subunit (β residues 1,302 and 1,305 to 1,306) at the mouth of the RNA-exit channel (Fig. 5 *A*–*D*).

There is an almost one-for-one correlation between the Qλ residues that undergo the disorder-to-order transition to form the Qλ torus upon NusA binding (residues 1 to 44) and the Qλ residues deleted in a deletion mutant defective in Qλ-dependent antitermination but not defective in Qλ-QBE and Qλ-RNAP interactions [residues 1 to 38 (17); Fig. 5*D*, pink ribbon]. There also is a correlation between Qλ residues that form the Qλ torus and Qλ residues altered in single-substitution mutants defective in Qλ-dependent antitermination but not defective in Qλ-QBE interaction [V6A and G39A (35); Fig. 5*D*, pink surfaces]. We conclude that the Qλ torus is functionally significant for Qλ-dependent antitermination.

The binding of the Q torus at the mouth of, and inside, the RNAP RNA-exit channel markedly restricts the RNAP RNA-exit channel, narrowing and extending the channel (Fig. 5 *E* and *F*). The Q-torus opening has a solvent-excluded diameter of just 5 to 7 Å (Fig. 5*E*). The presence of the Q torus at, and inside, the mouth of the RNAP RNA-exit channel does not affect accommodation of an 11-nt RNA product (Fig. 5 *A* and *F*), but would necessitate longer RNA products to thread through the Q-torus opening.

The Qλ torus in the structural state in Fig. 5 has no sequence, secondary-structure, or tertiary-structure similarity to the Q21 torus in structures of the Q21-loading complex and Q21-loaded complex (12, 16). However, the Qλ-torus opening has the same diameter as the Q21-torus opening [solvent-excluded diameter of 5 to 7 Å; Fig. 5*E* (12, 16)], the Qλ torus extends the same distance into the RNAP RNA-exit channel as the Q21 torus [accommodating a maximum of 11 to 13 nt of RNA before threading of RNA through the torus; Fig. 5 *E* and *F* (12)], and the Qλ torus has the same high net positive charge as the Q21 torus, enabling threading of RNA through interactions solely with the negatively charged RNA phosphate backbone [net positive charge of +4, excluding side chains that interact with RNAP (12)]. Thus, in the structural state in Fig. 5, Qλ forms a nozzle at, and inside, the RNAP RNA-exit channel that is not

homologous to, but that is analogous in all functionally important respects to, the nozzle previously observed in the Q21-loading complex and Q21-loaded complex.

We term the structural state in Fig. 5 the "Qλ 'engaged' loading complex" to reflect the fact that this structural state not only has Qλ recruited to the pTEC but also has Qλ reorganized to form a molecular nozzle interacting with, and entering, the RNAP RNA-exit channel.

Discussion

Qλ: Mechanism of Loading onto RNAP. The functional importance of the interactions between Qλ and the RNAP FTH that are observed in our structure of the pre-engaged Qλ-loading complex, but that are not observed in our structure of the NusA-containing engaged Qλ-loading complex, is validated by the finding that substitution of Qλ and FTH residues that make those interactions results in a specific defect in Qλ-dependent antitermination [Fig. 4*E*, red and green (23, 35)] and by the further finding that substitution of FTH residues that make those interactions results in a specific defect in Qλ-FTH interaction [Fig. 4*E*, green (23)]. The functional importance of the interactions between the Qλ torus and the RNAP RNA-exit channel that are observed in our structure of the NusA-containing engaged Qλ-loading complex, but that are not observed in our structure of the pre-engaged Qλ-loading complex, is validated by the finding that deletion or substitution of residues that make those interactions results in a specific defect in Qλ-dependent antitermination [Fig. 5*D*, pink ribbon and pink surfaces (17, 35)]. We conclude that *both* the pre-engaged Qλ-loading complex and the NusA-containing engaged Qλ-loading complex are bona fide, on-pathway intermediates in Qλ loading. We propose that Qλ loading involves two stages: 1) recruitment of Qλ, yielding a pre-engaged Qλ-loading complex, and 2) reorganization of Qλ to form a Qλ torus and engage the RNAP RNA-exit channel, yielding an engaged Qλ-loading complex. We propose further that NusA facilitates the transition from the pre-engaged Qλ-loading complex to the engaged Qλ-loading complex.

Comparison of the structure of the preengaged Qλ-loading complex at λPR′ (Fig. 4) to the structure of a Qλ-free pTEC at λPR′ (24), together with consideration of functional data for Qλ-RNAP interaction (21, 23, 35), indicates that formation of the pre-engaged Qλ-loading complex from the Qλ-free pTEC involves the following events: 1) binding of Qλ to the QBE; 2) repositioning of σR4 to the DNA segment upstream of σR2 bound to the SDPE -10-like element, displacing σR3 from the DNA segment; 3) bending of the DNA segment between the QBE and the pTEC by ∼40°, enabling interaction of the Qλ body with the RNAP ZBD; 4) folding of 16 residues at the Qλ N terminus and refolding of 12 residues at the Qλ C terminus; and 5) interaction of the Qλ N- and C-terminal segments with the RNAP FTH (Fig. 6 *A*, *Left*).

Comparison of the structure of the NusA-containing engaged Qλ-loading complex at λPR′ (Fig. 5) to the structure the pre-engaged Qλ-loading complex at λPR′ (Fig. 4), together with consideration of functional data for Qλ-dependent antitermination (17, 35), indicates that formation of the NusA-containing engaged Qλ-loading complex from the pre-engaged Qλ-loading complex involves the following events: 1) binding of NusA to Qλ and RNAP, making interactions with the Qλ body and RNAP α-subunit C-terminal domain and thus stabilizing the association between Qλ and RNAP; 2) interaction of the NusA N-terminal domain with the RNAP FTH, disrupting interactions between Qλ and the FTH and repositioning the FTH outside of and away from the RNAP RNA-exit channel; and 3) folding of 44 additional residues at the Qλ N terminus to form a Qλ torus that enters the RNAP RNA-exit channel (Fig. 6 *A*, *Right*).

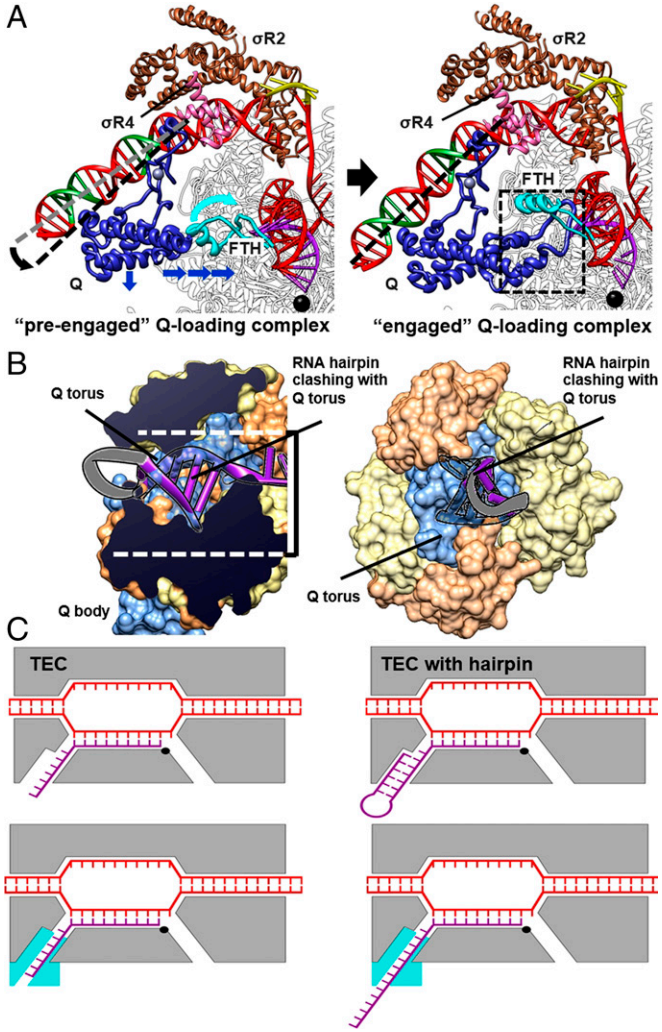

Fig. 6. Mechanistic conclusions. (*A*) Transformation of the pre-engaged Qλ-loading complex to the NusA-containing engaged Qλ-loading complex (NusA not shown for clarity). Black and gray dashed lines, DNA-helix axes of upstream double-stranded DNA segments in pre-engaged and engaged complexes, respectively; blue arrows, cyan arrow, and dashed rectangle, structural changes upon transformation of the pre-engaged complex to the engaged complex. Other colors are as in Figs. 4*B* and 5*A*. (*B*) Antitermination and antipausing by Qλ. Steric incompatibility of the Qλ torus with pause and terminator RNA hairpins (hairpin stem from PDB: 6ASX (57) as purple ribbon, with segments positioned to interpenetrate the Qλ torus indicated as transparent ribbons with black outlines; hairpin loop from PDB: 1MT4 (58) as gray ribbon with black outlines). View orientations and colors are as in Figs. 4*F* and 5*E*. (*C*) Schematic comparison of TECs in the absence of Qλ (upper row) and TECs in the presence of Qλ (lower row). Colors are as in Figs. 4*B* and 5*A*.

The inferred events in Qλ loading include a remarkable "two-handoff" mechanism. In formation of the pre-engaged Qλ-loading complex, the first handoff occurs: i.e., the RNAP FTH is handed from σR4—which interacts with the RNAP FTH in the absence of Qλ (25–28, 30, 31, 45)—to Qλ. In formation of the NusA-containing engaged Qλ-loading complex, the second handoff occurs: i.e., the FTH is handed from Qλ to NusA.

Whereas Qλ employs a NusA-dependent, two-stage process for Q loading—involving recruitment of Q to form a pre-engaged loading complex, followed by NusA-facilitated refolding of Q to form an engaged loading complex with a Q torus in the RNAP RNA-exit channel—Q21 loading occurs in a NusA-independent, single-stage process (12, 16). Nevertheless, Q21 loading shows a fundamental underlying analogy to Qλ

loading. The Q21-QBE complex and Q21-loading complex each contains two Q21 protomers, Q21u and Q21d, where "u" denotes upstream and "d" denotes downstream (12, 16). Q21u makes interactions analogous to those made by Qλ in the NusA-containing engaged Qλ-loading complex, interacting with the RNAP ZBD and forming a Q torus that enters the RNAP RNA-exit channel. Q21d makes interactions analogous to those made by NusA in the NusA-containing engaged Qλ-loading complex, interacting with Q21u and interacting with and repositioning the RNAP FTH. Thus, together, Q21u and Q21d make interactions analogous to the key Qλ-RNAP, Qλ-NusA, and NusA-RNAP interactions in the NusA-containing engaged Qλ-loading complex.

Qλ: Mechanisms of Antitermination and Antipausing. The structure of the NusA-containing engaged Qλ-loading complex immediately suggests the mechanisms of antipausing and antitermination by Qλ (Figs. 5 *E* and *F* and 6 *B* and *C*). RNA hairpin-dependent transcription pausing and transcription termination involve nucleation of an RNA hairpin at the mouth of the RNAP RNA-exit channel, followed by propagation of the RNA hairpin stem and penetration of the RNA hairpin stem into the RNAP RNA-exit channel (46, 47). The structure of the NusA-containing engaged Qλ-loading complex shows that Qλ is positioned to pose a steric barrier to nucleation, propagation, and penetration of the RNA-exit channel by a pause or terminator hairpin (Fig. 6 *B* and *C*). The Qλ torus is positioned to overlap, in toto, 4 to 5 bp of the stem of a pause or terminator hairpin, and thus is positioned to block propagation and penetration of the RNA-exit channel by a hairpin (Fig. 6 *B* and *C*). Because the Qλ torus has dimensions that accommodate only single-stranded RNA, the Qλ torus constitutes an effectively absolute steric barrier to the formation of the double-stranded RNA secondary structure at the mouth of, or inside, the RNAP RNA-exit channel (Fig. 6 *B* and *C*).

The structure of the NusA-containing engaged Qλ-loading complex suggests that Qλ also may exert antipausing activity by inhibiting RNAP swiveling—a rotation, by ∼3°, of the RNAP swivel module, comprising the RNAP ZBD and associated RNAP domains, that has been proposed to be associated with pausing [*SI Appendix*, Fig. S8 (38, 39, 48–50)]. In the structure of the NusA-containing engaged Qλ-loading complex, the RNAP swivel module is in the unswiveled state (*SI Appendix*, Fig. S8*A*), despite the presence of NusA, which favors the swiveled state (44). Model building indicates that interaction of the Qλ body with one face of the RNAP ZBD and the interaction of an α-helix of the Qλ torus with the other face of the RNAP ZBD would sterically preclude both the ∼3° swiveling associated with hairpin-dependent pausing (38, 39) and NusA binding (44) and the smaller, ∼1.5°, swiveling associated with elemental pausing [(38); *SI Appendix*, Fig. S8].

The structure of the NusA-containing engaged Qλ-loading complex implies that upon further RNA extension, RNA would thread into, and through, the Qλ torus (Figs. 5 *E* and *F* and 6 *B* and *C*). Because rethreading of the extruded RNA would be difficult or impossible, especially after RNA folding, threading of RNA through the Qλ torus would result in a topological linkage between RNA and Qλ, creating an essentially unbreakable linkage between the TEC and Qλ, enabling processive antitermination and antipausing over tens of thousands of nucleotide-addition steps (11).

The structures of this work indicate that the Qλ torus, like the Q21 torus (12, 16), forms a molecular nozzle that narrows and extends the RNAP RNA-exit channel, preventing the formation of pause and terminator hairpins, and that blocks formation of the RNAP swiveled state associated with pausing (Fig. 6*C* and *SI Appendix*, Fig. S8*B*).

Qλ and Q21: Functional Analogy without Structural Homology. Our results show that Qλ exhibits no three-dimensional structural similarity to Q21 [Figs. 2–5 (12, 16)], Qλ employs a different mechanism for DNA binding than Q21 [Fig. 3 (12, 16)], and Qλ employs a different, more complex, process of loading onto TECs than Q21 [Figs. 4–6 (12, 16)]. Nevertheless, our results indicate that Qλ employs the same molecular-nozzle mechanism for antipausing and antitermination as Q21 [Figs. 5 and 6 (12, 16)]. We conclude that Qλ and Q21 are not structural homologs and are solely functional analogs.

Prospect. One priority for further research is to determine whether the third protein family of lambdoid bacteriophage Q proteins, the Q82 protein family, also functions through a nozzle mechanism. The observation that Q82 can load onto a TEC that contains a long RNA product (51)—which should be topologically difficult or impossible for a factor functioning as a closed molecular nozzle—raises the possibility that Q82 might not function as a closed molecular nozzle.

Another priority for further research emerges from the hypothesis that nozzle formation by Q inhibits termination by extending the RNAP RNA-exit channel. The hypothesis implies that the same nozzle formation that prevents termination at standard terminators that contain a hairpin immediately followed by a 7- to 9-nt U-tract (46, 47) potentially could induce termination at nonstandard, "Q-dependent" terminators that contain a hairpin, followed by a spacer—an extension matching the extension of the RNAP RNA-exit channel—followed by a 7- to 9-nt U-tract [discussion in (7)]. In principle, such nonstandard, Q-dependent terminators could have functional roles in ending processive Q-dependent antitermination. Construction and analysis of libraries of terminator derivatives containing spacers between the hairpin and the U-tract, combined with analysis of corresponding sequences in bacteriophage or bacterial genomes, could address whether such nonstandard, Q-dependent terminators exist and, if so, whether they play functional roles.

Materials and Methods

Crystal structures of Qλ were solved by use of molecular replacement (53). The crystal structures of the Qλ-QBE complex were solved by use of experimental phasing with single-wavelength anomalous dispersion molecular replacement (54). Cryo-EM structures of the pre-engaged Qλ-loading complex and the NusA-containing engaged Qλ-loading complex were determined by use of single-particle reconstruction (55). Full details of methods are presented in *SI Appendix, SI Materials and Methods*.

Data, Materials, and Software Availability. Atomic coordinates and structure factors have been deposited in the Protein Data Bank (PDB) (accession nos. PDB 6VEU, PDB 6VEV, PDB 6VEW, PDB 6VEX, and PDB 6VEY) (59–63), and the Electron Microscopy Data Bank (EMDB) (accession nos. EMD-21158 and EMD-21159) (64, 65). All other study data are included in the article and/or supporting information.

ACKNOWLEDGMENTS. This work was supported by NIH Grants GM118059 (to B.E.N.) and GM041376 (to R.H.E.). We thank the Argonne National Laboratory for beamline access, the Rutgers Cryo-EM and Nanoimaging Facility and the National Center for CryoEM Access and Training (supported by NIH Grant GM129539, Simons Foundation Grant SF349247, and New York state grants) for microscope access, and J. Roberts for plasmids.

1. J. W. Roberts, Transcription termination and late control in phage lambda. *Proc. Natl. Acad. Sci. U.S.A.* **72**, 3300–3304 (1975).
2. E. J. Grayhack, J. W. Roberts, The phage lambda Q gene product: Activity of a transcription antiterminator *in vitro*. *Cell* **30**, 637–648 (1982).
3. E. J. Grayhack, X. J. Yang, L. F. Lau, J. W. Roberts, Phage lambda gene Q antiterminator recognizes RNA polymerase near the promoter and accelerates it through a pause site. *Cell* **42**, 259–269 (1985).
4. W. S. Yarnell, J. W. Roberts, The phage lambda gene Q transcription antiterminator binds DNA in the late gene promoter as it modifies RNA polymerase. *Cell* **69**, 1181–1189 (1992).
5. B. Z. Ring, J. W. Roberts, Function of a nontranscribed DNA strand site in transcription elongation. *Cell* **78**, 317–324 (1994).
6. B. Z. Ring, W. S. Yarnell, J. W. Roberts, Function of *E. coli* RNA polymerase sigma factor sigma 70 in promoter-proximal pausing. *Cell* **86**, 485–493 (1996).
7. W. S. Yarnell, J. W. Roberts, Mechanism of intrinsic transcription termination and antitermination. *Science* **284**, 611–615 (1999).
8. J. W. Roberts *et al.*, Antitermination by bacteriophage lambda Q protein. *Cold Spring Harb. Symp. Quant. Biol.* **63**, 319–325 (1998).
9. R. A. Weisberg, M. E. Gottesman, Processive antitermination. *J. Bacteriol.* **181**, 359–367 (1999).
10. J. W. Roberts, S. Shankar, J. J. Filter, RNA polymerase elongation factors. *Annu. Rev. Microbiol.* **62**, 211–233 (2008).
11. P. Deighan, A. Hochschild, The bacteriophage lambdaQ anti-terminator protein regulates late gene expression as a stable component of the transcription elongation complex. *Mol. Microbiol.* **63**, 911–920 (2007).
12. Z. Yin, J. T. Kaelber, R. H. Ebright, Structural basis of Q-dependent antitermination. *Proc. Natl. Acad. Sci. U.S.A.* **116**, 18384–18390 (2019).
13. H. C. Guo, M. Kainz, J. W. Roberts, Characterization of the late-gene regulatory region of phage 21. *J. Bacteriol.* **173**, 1554–1560 (1991).
14. W. Yarnell, "Interaction of the antitermination factor Q with complexes of RNA polymerase and DNA," PhD dissertation, Cornell University (1993).
15. X. J. Yang, J. A. Goliger, J. W. Roberts, Specificity and mechanism of antitermination by Q proteins of bacteriophages lambda and 82. *J. Mol. Biol.* **210**, 453–460 (1989).
16. J. Shi *et al.*, Structural basis of Q-dependent transcription antitermination. *Nat. Commun.* **10**, 2925 (2019).
17. S. M. Vorobiev *et al.*, Structure of the DNA-binding and RNA-polymerase-binding region of transcription antitermination factor λQ. *Structure* **22**, 488–495 (2014).
18. J. Guo, J. W. Roberts, DNA binding regions of Q proteins of phages λ and phi80. *J. Bacteriol.* **186**, 3599–3608 (2004).
19. C. Andreini, I. Bertini, G. Cavallaro, Minimal functional sites allow a classification of zinc sites in proteins. *PLoS One* **6**, e26325 (2011).
20. E. Bartlett, "Characterization of the functional interaction between the bacteriophage λ Q antiterminator and late gene promoter DNA," PhD dissertation, Cornell University (1998).
21. B. E. Nickels *et al.*, The interaction between σ^{70} and the β-flap of *Escherichia coli* RNA polymerase inhibits extension of nascent RNA during early elongation. *Proc. Natl. Acad. Sci. U.S.A.* **102**, 4488–4493 (2005).
22. B. E. Nickels, C. W. Roberts, J. W. Roberts, A. Hochschild, RNA-mediated destabilization of the σ^{70} region 4/β flap interaction facilitates engagement of RNA polymerase by the Q antiterminator. *Mol. Cell* **24**, 457–468 (2006).
23. P. Deighan, C. M. Diez, M. Leibman, A. Hochschild, B. E. Nickels, The bacteriophage λ Q antiterminator protein contacts the β-flap domain of RNA polymerase. *Proc. Natl. Acad. Sci. U.S.A.* **105**, 15305–15310 (2008).
24. C. Pukhrambam *et al.*, Structural and mechanistic basis of σ dependent transcriptional pausing. *Proc. Natl. Acad. Sci. USA* **119**, e2201301119 (2022).
25. D. G. Vassylyev *et al.*, Crystal structure of a bacterial RNA polymerase holoenzyme at 2.6 A resolution. *Nature* **417**, 712–719 (2002).
26. K. S. Murakami, S. Masuda, E. A. Campbell, O. Muzzin, S. A. Darst, Structural basis of transcription initiation: An RNA polymerase holoenzyme-DNA complex. *Science* **296**, 1285–1290 (2002).
27. V. Mekler *et al.*, Structural organization of bacterial RNA polymerase holoenzyme and the RNA polymerase-promoter open complex. *Cell* **108**, 599–614 (2002).
28. K. Kuznedelov *et al.*, A role for interaction of the RNA polymerase flap domain with the σ subunit in promoter recognition. *Science* **295**, 855–857 (2002).
29. D. A. Siegele, J. C. Hu, W. A. Walter, C. A. Gross, Altered promoter recognition by mutant forms of the σ^{70} subunit of *Escherichia coli* RNA polymerase. *J. Mol. Biol.* **206**, 591–603 (1989).
30. Y. Zuo, T. A. Steitz, Crystal structures of the *E. coli* transcription initiation complexes with a complete bubble. *Mol. Cell* **58**, 534–540 (2015).
31. B. Bae, A. Feklistov, A. Lass-Napiorkowska, R. Landick, S. A. Darst, Structure of a bacterial RNA polymerase holoenzyme open promoter complex. *eLife* **4**, e08504 (2015).
32. M. T. Marr, S. A. Datwyler, C. F. Meares, J. W. Roberts, Restructuring of an RNA polymerase holoenzyme elongation complex by lambdoid phage Q proteins. *Proc. Natl. Acad. Sci. U.S.A.* **98**, 8972–8978 (2001).
33. B. E. Nickels, C. W. Roberts, H. Sun, J. W. Roberts, A. Hochschild, The σ^{70} subunit of RNA polymerase is contacted by the λQ antiterminator during early elongation. *Mol. Cell* **10**, 611–622 (2002).
34. P. G. Devi, E. A. Campbell, S. A. Darst, B. E. Nickels, Utilization of variably spaced promoter-like elements by the bacterial RNA polymerase holoenzyme during early elongation. *Mol. Microbiol.* **75**, 607–622 (2010).
35. J. Guo, "Analysis of the functional domains and characterization of the DNA-binding domain of phage λ Q protein," PhD dissertation, Cornell University (1999).
36. R. S. Washburn, M. E. Gottesman, Regulation of transcription elongation and termination. *Biomolecules* **5**, 1063–1078 (2015).
37. G. A. Belogurov, I. Artsimovitch, Regulation of transcript elongation. *Annu. Rev. Microbiol.* **69**, 49–69 (2015).
38. J. Y. Kang *et al.*, RNA polymerase accommodates a pause RNA hairpin by global conformational rearrangements that prolong pausing. *Mol. Cell* **69**, 802–815.e5 (2018).
39. X. Guo *et al.*, Structural basis for NusA stabilized transcriptional pausing. *Mol. Cell* **69**, 816–827.e4 (2018).
40. F. Krupp *et al.*, Structural basis for the action of an all-purpose transcription anti-termination factor. *Mol. Cell* **74**, 143–157.e5 (2019).
41. C. Wang *et al.*, Structural basis of transcription-translation coupling. *Science* **369**, 1359–1365 (2020).
42. N. Said *et al.*, Steps toward translocation-independent RNA polymerase inactivation by terminator ATPase ρ. *Science* **371**, eabd1673 (2021).
43. Z. Hao *et al.*, Pre-termination transcription complex: Structure and function. *Mol. Cell* **81**, 281–292.e8 (2021).
44. C. Zhu *et al.*, Transcription factors modulate RNA polymerase conformational equilibrium. *Nat. Commun.* **13**, 1546 (2022).
45. K. S. Murakami, S. Masuda, S. A. Darst, Structural basis of transcription initiation: RNA polymerase holoenzyme at 4 A resolution. *Science* **296**, 1280–1284 (2002).
46. A. Ray-Soni, M. J. Bellecourt, R. Landick, Mechanisms of bacterial transcription termination. *Annu. Rev. Biochem.* **85**, 319–347 (2016).
47. J. W. Roberts, Mechanisms of bacterial transcription termination. *J. Mol. Biol.* **431**, 4030–4039 (2019).
48. J. Y. Kang, T. V. Mishanina, R. Landick, S. A. Darst, Mechanisms of transcriptional pausing in bacteria. *J. Mol. Biol.* **431**, 4007–4029 (2019).
49. G. A. Belogurov, I. Artsimovitch, The mechanisms of substrate selection, catalysis, and translocation by the elongating RNA polymerase. *J. Mol. Biol.* **431**, 3975–4006 (2019).
50. R. Landick, Transcriptional pausing as a mediator of bacterial gene regulation. *Annu. Rev. Microbiol.* **75**, 291–314 (2021).
51. C. D. Wells, P. Deighan, M. Brigham, A. Hochschild, Nascent RNA length dictates opposing effects of NusA on antitermination. *Nucleic Acids Res.* **44**, 5378–5389 (2016).
52. S. Shankar, A. Hatoum, J. W. Roberts, A transcription antiterminator constructs a NusA-dependent shield to the emerging transcript. *Mol. Cell.* **27**, 914–927 (2007).
53. M. G. Rossmann, The molecular replacement method. *Acta Crystallogr. A* **46**, 73–82 (1990).
54. B. C. Wang, Resolution of phase ambiguity in macromolecular crystallography. *Methods Enzymol.* **115**, 90–112 (1985).
55. Y. Cheng, Single-particle cryo-EM-How did it get here and where will it go. *Science* **361**, 876–880 (2018).
56. R. Albright, B. Matthews, 6CRO, Crystal structure of lambda-cro bound to a consensus operator at 3.0 angstrom resolution. PDB. https://www.rcsb.org/structure/6CRO. Accessed 27 July 2022.
57. J. Kang, R. Landick, S. Darst, 6ASX, CryoEM structure of E. coli his pause elongation complex. PDB. https://www.rcsb.org/structure/6ASX. Accessed 27 July 2022.
58. I. Lebars, *et al.*, 1MT4, Structure of 23S ribosomal RNA hairpin 35. PDB. https://www.rcsb.org/structure/1MT4. Accessed 27 July 2022.
59. Z. Yin, R. H. Ebright, 6VEU, Transcription antitermination factor Qlambda, type-I crystal. PDB. https://www.rcsb.org/structure/unreleased/6VEU. Deposited 1 March 2020.
60. Z. Yin, R. H. Ebright, 6VEV, Transcription antitermination factor Qlambda, type-II crystal. PDB. https://www.rcsb.org/structure/unreleased/6VEV. Deposited 1 March 2020.
61. Z. Yin, R. H. Ebright, 6VEW, Transcription antitermination factor Qlambda in complex with Qlambda-binding-element DNA. PDB. https://www.rcsb.org/structure/unreleased/6VEW. Deposited 1 March 2020.
62. Z. Yin, R. H. Ebright, 6VEX, Transcription antitermination complex: "pre-engaged" Qlambda-loading complex. PDB. https://www.rcsb.org/structure/unreleased/6VEX. Deposited 1 March 2020.
63. Z. Yin, R. H. Ebright, 6VEY, Transcription antitermination complex: NusA-containing "engaged" Qlambda-loading complex. PDB. https://www.rcsb.org/structure/unreleased/6VEY. Deposited 1 March 2020.
64. Z. Yin, R. H. Ebright, EMD-21158, Transcription antitermination complex: "pre-engaged" Qlambda-loading complex. EMDB. https://www.ebi.ac.uk/emdb/EMD-21158. Deposited 1 March 2020.
65. Z. Yin, R. H. Ebright, EMD-21159, Transcription antitermination complex: NusA-containing "engaged" Qlambda-loading complex. EMDB. https://www.ebi.ac.uk/emdb/EMD-21159. Deposited 1 March 2020.